



OPEN Early hemodynamic differences between generalized and focal epilepsy measured by photoplethysmography

Aoxue Mei^{1,5}, Cong Fu^{1,5}, Zhao Liu¹, Yujiao Yang², Xiongfei Wang¹, Mengyang Wang², Jing Wang², Zhigang Han⁴, Yujie Bo¹, Ke Xu¹, Chongyang Tang¹ & Guoming Luan^{1,3}✉

Photoplethysmography (PPG) detects hemodynamic changes during epileptic seizures. This study aims to investigate PPG signal changes during generalized tonic-clonic seizures (GTCSs) and focal impaired awareness seizures (FIASs). 17 GTCS and 19 FIAS episodes were recorded from 18 patients. The 30 min preictal period was divided into three 10-minute intervals. PPG features analyzed were pulse upslope (PUS), maximal compliance (Kmax), and skewness. Features across 3 preictal intervals showed significant reductions compared to the baseline: PUS ($F_{(3,64)} = 11.870, p < 0.001$), Kmax ($F_{(3,64)} = 7.419, p < 0.001$) and skewness ($F_{(3,64)} = 2.852, p = 0.044$) in the GTCS group. PUS (Kruskal–Wallis [$K-W$] = 22.600, $p < 0.001$) and Kmax ($K-W = 28.110, p < 0.001$) in the FIAS group. In the GTCS group, the largest difference was observed 30 min before seizure onset (PUS: $p < 0.001$, Cohen's $d = 1.843$; Kmax: $p < 0.001$, Cohen's $d = 1.419$; skewness: $p = 0.043$, Cohen's $d = 0.808$), whereas this was not the case in the FIAS group. PPG signals showed earlier changes in the GTCS group than in the FIAS group, highlighting their differences and the potential of PPG-based monitoring for early seizure detection.

Keywords Epilepsy, Photoplethysmography, Generalized tonic-clonic seizures, Focal impaired awareness seizures

Epilepsy is a common neurological disorder that affects approximately 50 million people worldwide and significantly impairs their quality of life¹. Epilepsy comprises various seizure types, including generalized tonic-clonic seizures (GTCSs) and focal impaired awareness seizures (FIASs), each of which presents distinct clinical challenges. FIASs are often underdiagnosed due to their subtle clinical manifestations², whereas GTCSs pose immediate physical risks, including sudden unexpected death in epilepsy (SUDEP)³. Owing to the clinical complexity of epilepsy and its diverse manifestations, identifying effective and reliable methods for early seizure detection is crucial for facilitating early diagnosis and optimizing clinical management⁴.

Electroencephalography (EEG) remains the gold standard for seizure detection; however, its dependence on bulky, nonportable equipment limits its feasibility for continuous, real-world monitoring. To overcome this problem, wearable alternatives, including accelerometry (ACC), photoplethysmography (PPG) and electrocardiography (ECG), have been investigated; among these methods, ACC frequently produces a high false alarm rate, up to 5.7 false alarms per 24 h⁵. ECG is a well-established tool for assessing autonomic nervous system (ANS) function, particularly through heart rate (HR) and heart rate variability (HRV), but it is limited in its ability to directly capture peripheral vascular dynamics and microcirculatory regulation, which are also affected during seizures^{6,7}. On the contrary, widely integrated into medical devices for autonomic function assessment, PPG enables the measurement of parameters such as oxygen saturation, cardiac output, heart rate, microcirculatory regulation and vascular dynamics⁸. As a result, it has been positioned as a promising tool to detect physiological alterations associated with epileptic seizures^{7,9–12}. Seizures, especially during the preictal period, are frequently associated with fluctuations in these physiological parameters¹³. Among these changes, HRV and vascular tone alterations have been identified as reliable physiological markers for automated seizure detection¹⁴. Furthermore, PPG has demonstrated its ability to capture seizure-induced cardiovascular changes,

¹Department of Neurosurgery, Sanbo Brain Hospital, Capital Medical University, No. 50 Xiang Shan Yi-Ke-Song Road, Haidian District, Beijing 100093, China. ²Department of Neurology, Sanbo Brain Hospital, Capital Medical University, Beijing 100093, China. ³Laboratory for Clinical Medicine, Capital Medical University, Beijing 100069, China. ⁴Beijing Zhengqihe Health Technology Co., Ltd, No. 103, Building 2, North Qing Road, Haidian District, Beijing 100089, China. ⁵Aoxue Mei and Cong Fu contributed equally to this work. ✉email: luangm@ccmu.edu.cn

reinforcing its potential as a valuable tool for early seizure detection and monitoring¹⁵. This observation suggests that PPG signals may serve as a noninvasive modality for detecting autonomic fluctuations preceding seizure onset, potentially enabling real-time seizure prediction.

Previous studies^{9,16–19} have demonstrated the potential of PPG-based seizure detection in clinical settings. However, most investigations have focused on either GTCs or FIAs in isolation, without direct comparisons or comprehensive analyses of raw PPG data. The aim of this study was to explore preictal differences in PPG-derived features between GTCs and FIAs, with a particular focus on autonomic dysregulation. Specifically, we analyze alterations in PPG-derived features across three distinct time points in the preictal phase and compare three PPG features (US, kmax, and skewness) to characterize their temporal variations. This study explores the potential of PPG-derived features as biomarkers of hemodynamic and ANS alterations in the preictal period, which may aid in improving noninvasive seizure monitoring.

To avoid ambiguity, we define “early seizure detection” in this study as the identification of physiological changes that occur prior to clinical or electrographic seizure onset, primarily within the preictal period²⁰. Although this aligns with the concept of seizure prediction, we retain the term “early detection” to emphasize its clinical goal and to remain consistent with related literature on wearable seizure monitoring. Many prior studies cited in this work focus on ictal-phase detection, but their findings regarding PPG dynamics remain highly relevant for understanding preictal hemodynamic changes.

Materials and methods

Patients

Patients were recruited from the epilepsy center at Sanbo Brain Hospital, where they underwent long-term video-EEG monitoring. The study protocol was approved by the institutional review board of Sanbo Brain Hospital, and written informed consent was obtained from all participants or their caregivers. This procedure ensured that each seizure event analyzed was independent and not part of a seizure cluster.

The inclusion criteria were as follows: Patients were classified according to the ILAE classification as primary or secondary GTCs or FIAs². To ensure seizure type classification consistency, each patient contributed episodes of only one seizure type; no individual experienced both GTCs and FIAs during the study. They had at least 30 min of artifact-free preictal PPG data, experienced at least one seizure while wearing the PPG sensors, and remained in a consistent resting state (e.g., seated or supine) during monitoring. The detailed exclusion criterion was as follows: patients with nonepileptic or comorbid neurological disorders. Patients who had taken medications affecting autonomic function (e.g., β -blockers, anticholinergics) within 48 h prior to data collection. All patients provided written informed consent (or their caregivers provided consent for minors or cognitively impaired individuals). This study focused on GTCs and FIAs, because they are among the most prevalent and clinically representative seizure types, and they exhibit distinct patterns of autonomic involvement. Furthermore, only these two seizure types had sufficient numbers of artifact-free, high-quality PPG recordings in our dataset to allow for meaningful comparative analysis. The recruitment process is illustrated in (Fig. 1). Patient information is shown in (Supplement Table 1).

All methods were performed in accordance with the relevant guidelines and regulations. The study was approved by the Ethics Committee of Sanbo Brain Hospital, Capital Medical University, and informed consent was obtained from all participants or their legal guardians.

EEG and PPG monitoring

Patients underwent continuous long-term video-EEG monitoring (NicoletOne LTM EEG) via standard scalp EEG montages based on the 10–20 system. The participants wore sensors on their left wrists (SHW-100, SungoHealth, China) during their stay to record PPG signals intermittently. The SHW-100 (SungoHealth, China) is a research-grade wrist-worn device equipped with a reflective green-light PPG sensor (wavelength: 526 nm). The device performs intermittent acquisition, recording short-duration PPG segments once every 10 min. To improve signal quality, the device includes onboard multi-stage filtering and real-time anomaly rejection algorithms. The SHW-100 has been employed in clinical research settings for long-term physiological monitoring, supporting its applicability in controlled experimental environments. Seizure types were categorized as GTCs, including both primary and secondary forms, or FIAs. Seizure onset and offset times were determined from the EEG data by two board-certified epileptologists with expertise in EEG interpretation, using standard clinical criteria and video-EEG correlation. Additionally, we excluded seizures that occurred within 90 min of a previous seizure, as these could be part of a continuous seizure cluster and may confound the analysis of preictal changes¹⁰. In the FIAS group, many patients experienced multiple seizures within short time intervals, and as a result, a large proportion of FIAS episodes were excluded based on this criterion.

PPG signal selection

To evaluate preictal changes and differentiate seizure-related alterations from normal physiological variations, PPG signals were analyzed across distinct preictal and baseline periods. These time intervals were selected based on prior studies^{10,11} on preictal autonomic changes and their clinical relevance for early seizure detection. The analyzed periods were defined as follows:

1. P1 (0–10 min before seizure onset): The 10-minute interval immediately preceding seizure onset.
2. P2 (10–20 min before seizure onset): The 10-minute interval spans 10 to 20 min preictally.
3. P3 (20–30 min before seizure onset): The 10-minute interval spans 20 to 30 min preictally.
4. Baseline (seizure-free baseline): Seizure-free, awake-state segments recorded at least 6 h before or after any seizure event served as a reference for distinguishing seizure-related changes from normal physiological fluctuations.

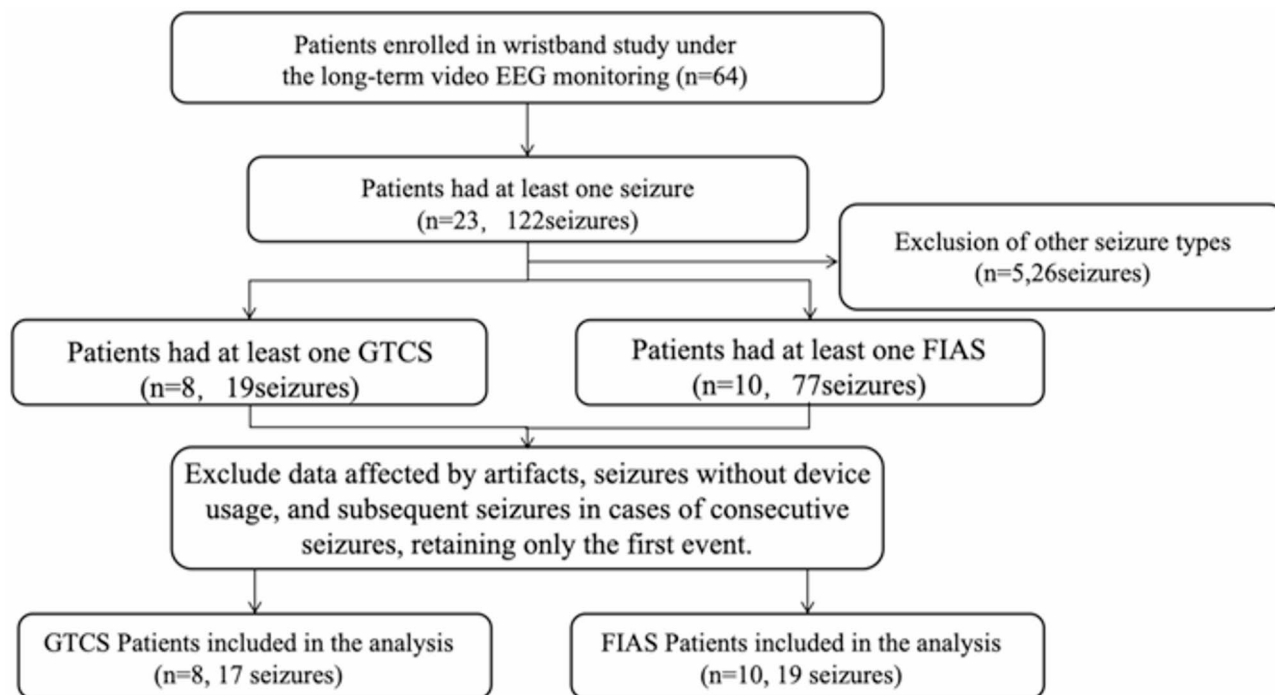


Fig. 1. Patient enrollment flowchart. *GTCSs* generalized tonic-clonic seizures, *FIASs* focal impaired awareness seizures, *PPG* photoplethysmography, *EEG* electroencephalography.

	GTCS (N=8)	FIAS (N=10)	Summary statistics	<i>p</i> - value
Gender: Male	3(37.50%)	4(40.00%)	–	1.000 [#]
Age	26.88 ± 4.50	18.80 ± 3.00	<i>t</i> = 1.88	0.23
Disease duration	16.00 ± 2.50	11.90 ± 4.50	<i>t</i> = 0.98	0.56
EEG onset-right-hemisphere	2(25.00%)	5(50.00%)	–	0.367 [#]
MRI finding-normal	5(62.50%)	2(20.00%)	–	0.145 [#]
MEG-right hemisphere	3(37.50%)	2(20.00%)	–	0.608 [#]
PET-CT-right hemisphere	2(25.00%)	2(20.00%)	–	1.000 [#]

Table 1. Clinical characteristics. *MEG* magnetoencephalography, *PET-CT* positron emission tomography-computed tomography, *Lt* left, *Rt* right, *Bl* bilateral, *HS* hippocampal sclerosis, *HH* hypothalamic hamartoma, *FCD* focal cortical dysplasia. [#]*Fisher's* precision probability test.

For each period, we selected 10-minute segments devoid of motion artifacts. To ensure data quality, segments contaminated by motion artifacts were manually excluded from the analysis. This segmentation approach established a reliable framework for identifying seizure-specific PPG signal changes and enabled robust analysis of preictal physiological variations.

PPG feature extraction

We used Python (version 3.11) for preprocessing, segmentation, and feature extraction of the PPG signals. Variational mode decomposition (VMD) was applied to preprocess the PPG signal^{21,22} (for the detailed methodology, please refer to the supplementary materials and Methods section). After decomposition, the central frequency of each mode was estimated, and modes with frequencies outside the physiologically relevant range (e.g., < 0.8 Hz or > 10 Hz) were discarded to retain only meaningful components related to hemodynamic responses and ANS activity. The denoised PPG signal was then reconstructed by summing the selected modes.

To increase the robustness of the extracted features and mitigate the influence of noise and motion artifacts, this study applied a one-sample Z-score approach to detect and remove outliers prior to peak detection. Specifically, individual Z-scores were calculated for each extracted feature value within the 10-minute segment, and values exceeding ± 3 standard deviations from the mean were excluded. This method effectively eliminated extreme values while preserving overall signal integrity. Following preprocessing and outlier removal, peak detection algorithms were applied to identify pulse wave peaks, which were then organized into a structured feature matrix for statistical analysis and classification. Although peak detection was used to facilitate the identification of pulse cycles, the full denoised and VMD-reconstructed PPG waveform was preserved

throughout the preprocessing pipeline. Key physiological features were then extracted from the denoised PPG signal to characterize hemodynamic responses and ANS activity. The extracted features included PUS, Kmax, and skewness.

PUS refers to the maximum slope of the rising phase of the PPG waveform, calculated as the peak of the first derivative. It is considered a morphology-based feature reflecting the dynamics of vascular tone and hemodynamic responses²³. The PUS is calculated as:

$$PUS = \max \left(\frac{dPPG(t)}{dt} \right)$$

where $PPG(t)$ represents the PPG signal at time t and where $\frac{dPPG(t)}{dt}$ denotes the first derivative of the PPG signal.

Kmax, derived from the second derivative of the PPG signal, was used to characterize arterial compliance. This interpretation is supported by recent modeling studies demonstrating that vascular compliance significantly shapes PPG waveform morphology through its influence on vascular tone and hemodynamic response²⁴. The Kmax is calculated as:

$$K_{max} = PPG \left(T : \frac{d^2 PPG(t)}{dt^2} = \min \left(\frac{d^2 PPG(t)}{dt^2} \right) \right)$$

where $PPG(t)$ represents the PPG signal at time t , $\frac{d^2 PPG(t)}{dt^2}$ is the second derivative of the PPG signal and T is the time at which the first local minimum of $\frac{d^2 PPG(t)}{dt^2}$ occurs.

Skewness is a metric used to assess the symmetry and quality of a signal. It also helps to detect motion artifacts, as asymmetry in the signal often reflects external disturbances or changes in the physiological state²⁵. Skewness is calculated as:

$$Skewness = \frac{\frac{1}{N} \sum_{i=1}^N (x_i - \bar{x})^3}{\left(\frac{1}{N} \sum_{i=1}^N (x_i - \bar{x})^2 \right)^{3/2}}$$

where x_i represents the i -th sample of the PPG signal, \bar{x} represents the mean value of the PPG signal, N represents the total number of samples, and S represents the skewness of the distribution, with $S > 0$ indicating a right-skewed waveform and $S < 0$ indicating a left-skewed waveform.

Statistical analysis

We used SPSS (version 26, IBM Corp., Armonk, NY, USA) for the statistical analysis. Descriptive statistics were computed for all variables, and normality was assessed via the Shapiro-Wilk test. Fisher's exact test was used for categorical variable comparisons, whereas continuous variables were analyzed via an independent samples t test. For within-group comparisons across time points, normally distributed variables were analyzed via one-way analysis of variance (ANOVA) with Bonferroni post hoc correction, and nonnormally distributed variables were analyzed via the Kruskal-Wallis (K-W) test with Dunn's post hoc correction. Effect sizes were reported via Cohen's d for post hoc comparisons where applicable. For between-group comparisons at each time point, normally distributed variables were assessed via the independent t test, and nonnormally distributed variables were analyzed via the Mann-Whitney U test.

Results

Patients

Ultimately, in all the enrolled 64 patients, 19 FIAS episodes from 10 patients (male: $n = 4$; age: 18.80 ± 3.00) and 17 GTCS episodes from 8 patients (male: $n = 3$; age: 26.88 ± 4.50) were included in the analysis. Table 1 presents the demographic and clinical information of the patients. The proportion of male patients was similar between the two groups, with 37.5% in the GTCS group and 40.0% in the FIAS group ($p = 1.00$). The mean age of the GTCS group was 26.88 ± 4.50 years, whereas the FIAS group had a lower mean age of 18.80 ± 3.00 years; however, the difference was not statistically significant ($t = 1.88$, $p = 0.23$). The average disease duration was 16.00 ± 2.50 years in the GTCS group and 11.90 ± 4.50 years in the FIAS group, with no significant difference observed ($t = 0.98$, $p = 0.56$). Regarding neurophysiological findings, EEG recordings indicated seizure onset in the right hemisphere in 25.0% of GTCS group and 50.0% of FIAS group. Similarly, magnetoencephalography (MEG) detected right-hemisphere abnormalities in 37.5% of GTCS group and 20.0% of FIAS group, whereas PET-CT findings revealed abnormalities in the right hemisphere in 25.0% of GTCS group and 20.0% of FIAS group.

Differences in PPG features

Compared with baseline, certain preictal intervals showed significantly lower feature values, as determined by Bonferroni-corrected post hoc comparisons: PUS ($F_{(3,64)} = 11.870$, $p < 0.001$), Kmax ($F_{(3,64)} = 7.419$, $p < 0.001$) and skewness ($F_{(3,64)} = 2.852$, $p = 0.044$) in the GTCS group. PUS (Kruskal-Wallis [K-W] = 22.600, $p < 0.001$) and Kmax (K-W = 28.110, $p < 0.001$) in the FIAS group. Intergroup comparison (GTCS vs. FIAS) revealed significant differences only at 30 min before seizure onset (Kmax: $U = 94$, $p = 0.033$; skewness: $U = 89$, $p = 0.021$).

Generalized tonic-clonic seizures

In the GTCS group, PUS and Kmax significantly changed in all three preictal periods compared with the baseline values: PUS (P3: *Cohen's d* = 1.843, $p < 0.001$; P2: *Cohen's d* = 1.296, $p = 0.001$; P1: *Cohen's d* = 1.422, $p < 0.001$) and Kmax (P3: *Cohen's d* = 1.419, $p < 0.001$; P2: *Cohen's d* = 1.116, $p = 0.007$; P1: *Cohen's d* = 1.092, $p = 0.005$). However, skewness demonstrated a marked difference only at P3 (*Cohen's d* = 0.043, $p = 0.043$). The effect size was greatest at P3, particularly for the PUS and Kmax features. The details are shown in (Table 2; Fig. 2A, C).

Focal impaired awareness seizures

In the FIAS group, only 2 features exhibited significant reductions across the three preictal intervals compared with baseline: PUS significantly decreased in P3 (*Cohen's d* = 1.020, $p < 0.001$), P2 (*Cohen's d* = 1.192, $p < 0.001$) and P1 (*Cohen's d* = 1.101, $p < 0.001$). Kmax (P3: *Cohen's d* = 1.416, $p < 0.001$; P2: *Cohen's d* = 1.94, $p < 0.001$; P1: *Cohen's d* = 1.656, $p < 0.001$). However, the skewness did not significantly differ. The effect size was greatest at P2 for all three features compared with P1 and P3. The details are shown in (Table 2; Fig. 2B, D).

PPG feature comparisons of the GTCS and FIAS groups

The PPG features between the GTCS and FIAS groups were compared across different preictal periods. No significant differences in PUS were observed between the GTCS and FIAS groups at any time point (P3, P2, and P1), with p values of 0.573, 0.876, and 0.573, respectively. A significant difference in Kmax was identified between the GTCS and FIAS groups at P3 ($U = 94$, $p = 0.030$), whereas no significant differences were found at P2 ($p = 0.9$) or P1 ($p = 0.639$). A significant difference in skewness was observed at P3 ($U = 89$, $p = 0.020$), but no significant differences were noted at P2 ($p = 0.466$) or P1 ($p = 0.190$). These results indicate that there are certain differences in the PPG features, particularly the Kmax and skewness features, between the GTCS and FIAS groups at different time points. The details are shown in (Table 3; Fig. 3A, C).

	Mean \pm SD	95% CI	F/K-W	p	Cohen's d
GTCS-PUS					
Baseline	2429 \pm 518.6	2163–2696	11.87	–	–
P3	1083 \pm 659.4	745–1423		<0.001***	1.843
P2	1484 \pm 869	1037–1930		0.001**	1.296
P1	1391 \pm 687.2	1038–1744		<0.001***	1.422
GTCS-Kmax					
Baseline	35,903 \pm 9539	30,999–40,808	7.419	–	–
P3	18,797 \pm 11,269	13,003–24,591		<0.001***	1.419
P2	25,035 \pm 14,850	17,400–32,671		0.007**	1.116
P1	22,743 \pm 11,369	16,898–28,588		0.005**	1.092
GTCS-skewness					
Baseline	0.2243 \pm 0.0985	0.1736–0.2750	2.852	–	–
P3	0.1122 \pm 0.1397	0.04035–0.1840		0.043*	0.808
P2	0.1186 \pm 0.1859	0.023–0.2142		0.213	0.762
P1	0.1693 \pm 0.1017	0.1170–0.2216		0.9	0.396
FIAS-PUS					
Baseline	3093 \pm 943.5	2638–3548	22.6	–	–
P3	1848 \pm 1256	1243–2453		0.001**	1.02
P2	1653 \pm 1454	952.4–2354		<0.001***	1.192
P1	1756 \pm 1265	1146–2366		<0.001***	1.101
FIAS-Kmax					
Baseline	46,193 \pm 11,125	40,831–51,555	28.11	–	–
P3	28,503 \pm 13,076	22,201–34,805		<0.001***	1.416
P2	22,422 \pm 11,875	16,698–28,146		<0.001***	1.94
P1	25,715 \pm 12,750	19,570–31,861		<0.001***	1.656
FIAS-skewness					
Baseline	0.2376 \pm 0.043	0.2167–0.2586	7.361	–	–
P3	0.21 \pm 0.08	0.1712–0.2488		0.3298	0.306
P2	0.1853 \pm 0.1132	0.1307–0.2398		0.0549	0.581
P1	0.1984 \pm 0.096	0.1524–0.244		0.5241	0.431

Table 2. Within-group comparisons of PPG features across preictal periods F in the GTCS and FIAS groups. Statistical tests include one-way ANOVA (the F value indicates the ratio of variance between groups to variance within groups) with Bonferroni post hoc correction for the GTCS group and the Kruskal–Wallis test with Dunn's test for the FIAS group; Cohen's d indicates the effect size.

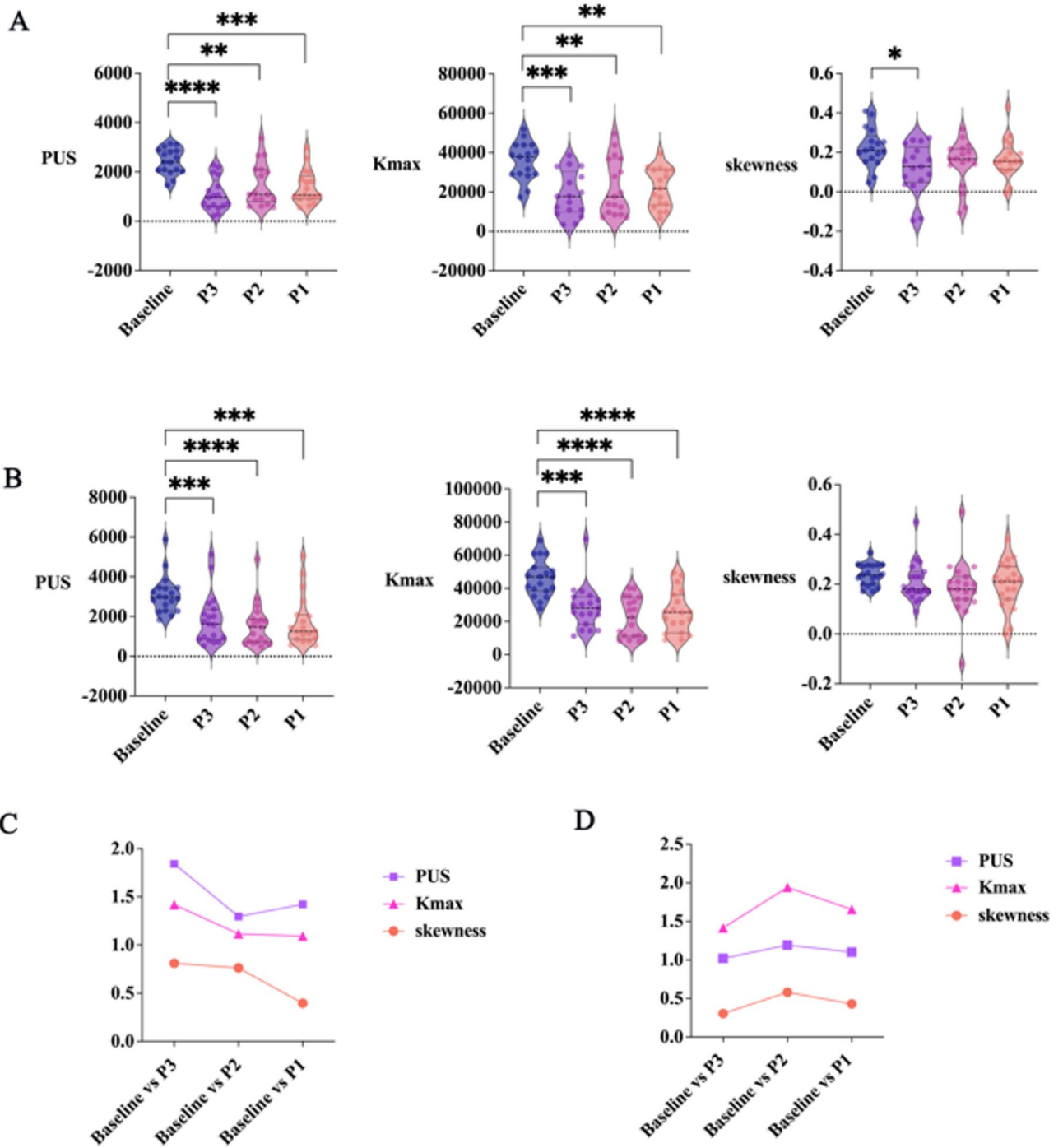


Fig. 2. Violin plots (A,B) and effect size plots (C,D) of PUS, Kmax, and skewness across preictal periods. (A,C) show results from the GTCS group; (B,D) show results from the FIAS group. Violin plots display the distribution of each feature across baseline and three preictal intervals (P3, P2, P1). Internal dashed lines indicate the median (central line) and the 25th/75th percentiles (outer lines). Statistical significance: **** $p < 0.0001$, *** $p < 0.001$, ** $p < 0.01$, * $p < 0.05$. Effect size plots illustrate the magnitude of differences (Cohen’s d) between baseline and each preictal period.

Discussion

This study highlights the hemodynamic alterations in GTCSs and FIAs via PPG feature detection. Compared with those at baseline, significant reductions in all three features (PUS, Kmax, and skewness) were observed during the preictal periods (P1, P2 and P3). The most pronounced PUS and Kmax changes were observed during GTCSs and FIAs; however, the changes in skewness were less consistent. Compared with that in the FIAS

Feature	Group (GTCS vs. FIAS)	<i>p</i>	Mann–Whitney U
PUS	P3	0.573	143
	P2	0.876	156
	P1	0.573	143
Kmax	P3	0.030*	94
	P2	0.900	157
	P1	0.639	146
Skewness	P3	0.020*	89
	P2	0.466	138
	P1	0.190	120

Table 3. Between-group comparison of PPG features across preictal periods in the GTCS and FIAS groups.

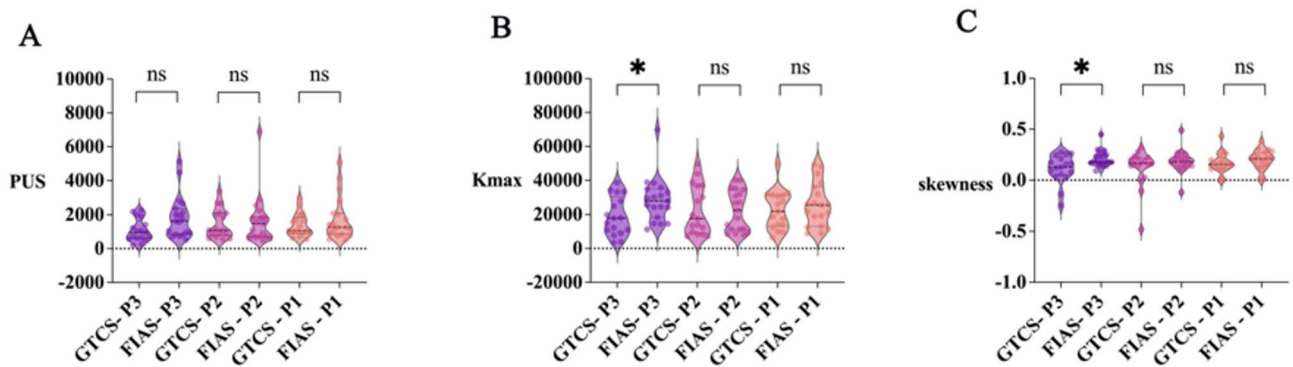


Fig. 3. Violin plots comparing PPG features between GTCS and FIAS groups across different preictal periods. Violin plots depict the distributions of PUS, Kmax, and skewness, respectively, across the preictal periods. The internal dashed lines represent the median (central line) and the 25th/75th percentiles (outer lines). At P3, significant differences in Kmax and skewness were observed between the GTCS and FIAS groups (Kmax: $U = 94$, $p = 0.030$; skewness: $U = 89$, $p = 0.020$). Statistical significance: * $p < 0.05$.

group, the PPG signal in the GTCS group exhibited earlier changes at 30 min before seizure onset. These findings suggest the potential for PPG-based monitoring to aid clinicians in the early detection of seizures.

Differences in the PPG features of GTCS and FIAS groups

ANS dysfunction in epilepsy has been well documented, particularly its impact on cardiovascular regulation²⁶. Eggleston KS et al.²⁷ has demonstrated that ictal events are associated with significant increases in HR in a large proportion of epilepsy patients (82%), as observed through concurrent EEG and ECG monitoring. These autonomic alterations may influence vascular tone, capillary perfusion, and blood flow dynamics, potentially contributing to the hemodynamic changes observed prior to seizure onset. Since PPG signals reflect key ANS-regulated functions such as HR, blood pressure, and vascular compliance, alterations in these signals may serve as early indicators of impending seizures^{10,11,28}. This study selected PUS, Kmax, and skewness based on their theoretical and empirical associations with hemodynamic and ANS regulation. Among these, PUS is the most well-established and interpretable, representing the steepness of the systolic upstroke and thereby reflecting changes in peripheral blood flow velocity, which is tightly linked to sympathetic activation and vascular tone. Kmax is a second-order derivative feature extracted from the PPG waveform and was used to characterize arterial compliance²⁴. Recent studies²⁹ have demonstrated that compliance-related changes in vascular tone significantly affect PPG waveform morphology, supporting its use in evaluating hemodynamic responses. Skewness, in contrast, is not a direct physiological parameter but rather a statistical descriptor of waveform asymmetry. While it may reflect waveform deformation due to motion artifacts, localized perfusion irregularities, or muscle activity, it is treated as a secondary, morphology-sensitive feature in our analysis and not a primary indicator of ANS function. Furthermore, although prior studies¹¹ have demonstrated that peak amplitude, area under the curve, and smoothness are valuable features in seizure detection, we opted not to include these in the current analysis to maintain focus on features with clearer ANS linkages and stronger temporal stability across preictal windows.

In this study, both the GTCS and FIAS groups presented significant reductions in PUS and Kmax, suggesting that ANS dysfunction is likely due to an imbalance between sympathetic and parasympathetic activity²⁶. In the GTCS group, the PPG signals exhibited earlier changes, with significant alterations observed as early as 30 min before seizure onset. Effect size analysis further confirmed this temporal distinction, showing that the peak effect size occurred at P3 in the GTCS group, whereas in the FIAS group, the peak effect size occurred at P2 instead

of P3. This difference may primarily result from the varying impacts of the two seizure types on the ANS³⁰. In the GTCS group, generalized epileptic discharge had a more extensive and intense regulatory effect on the ANS. This widespread discharge affects multiple ANS-related brain regions, such as the amygdala, anterior insula, anterior cingulate cortex, posterior orbitofrontal cortex, hypothalamus, periaqueductal gray, parabrachial region in the pons, solitary tract nucleus, and ventrolateral medulla, leading to widespread autonomic imbalance³¹. In contrast, the focal discharge in the FIAS group had a more restricted influence on the ANS, which was typically confined to specific brain regions, resulting in a milder alteration of autonomic function.

Across all preictal periods (P1, P2, and P3), significant reductions in PUS and Kmax were observed compared with those at baseline in both the GTCS and FIAS groups. Skewness exhibited less consistent changes, with a significant reduction observed only in the GTCS group during P3. However, since this time window precedes overt convulsive activity, the cause of the observed reduction in skewness remains unclear. Although skewness has been proposed as a motion-sensitive indicator²⁵, and differences in seizure semiology between GTCS and FIAS may indirectly contribute to variations in waveform asymmetry³². Nevertheless, whether skewness can reliably reflect waveform morphology changes induced by subtle autonomic dysfunction, hemodynamic shifts, or other physiological disturbances remains uncertain and warrants further investigation to clarify its physiological basis.

ANS as the physiological basis for PPG-based seizure detection

The ANS consists primarily of the SNS and the PNS, which exert opposing effects on cardiovascular function³⁰. SNS activation accelerates HR and induces peripheral vasoconstriction, consequently reducing the PPG signal amplitude³³. In contrast, PNS activation promotes vasodilation, increasing the PPG amplitude. The fluctuations in the PPG amplitude directly reflect blood volume dynamics and vascular tone regulation³⁴.

Previous research^{35–38} has demonstrated that autonomic dysfunction emerges during the preictal period, characterized by an increase in HR before EEG or clinical seizure onset. In some patients without overt clinical symptoms, HR changes may be the only detectable physiological abnormality. These findings suggest that HR could serve as a potential biomarker for early seizure detection, indicating that autonomic disturbances occur before seizure onset. While most previous studies^{12,16} have relied on PPG-derived HR data for monitoring and seizure detection, importantly, HR is only one factor influencing PPG signals. Our study extends beyond HR monitoring by analyzing raw PPG signals, revealing ANS changes that may support early seizure detection. These changes in ANS function are closely linked to the triggering mechanisms of seizures. Specifically, activation of the sympathetic nervous system leads to vasoconstriction, increased cardiac output, and elevated blood pressure, which results in reduced microcirculatory blood flow and decreased vascular compliance. Since PUS reflects the rate of increase in peripheral blood flow during each heartbeat, a decrease in PUS indicates reduced blood flow in the microcirculation, likely caused by an imbalance in the ANS. Similarly, Kmax, a morphology-based feature derived from the second derivative of the PPG waveform, may reflect changes in arterial compliance. The observed preictal decrease in Kmax may be attributed to reduced vascular compliance associated with autonomic dysfunction. Our findings suggest that PPG-derived features provide additional physiological insights beyond HR, offering a more comprehensive understanding of the autonomic changes surrounding seizure events. These insights may contribute to improving early seizure detection and offer further understanding of the role of ANS dysregulation in the pathophysiology of epilepsy.

Challenges and prospects of PPG-based seizure detection

The use of wrist-worn PPG signals as a peripheral monitoring tool for epilepsy offers significant advantages in terms of wearable convenience and long-term monitoring. Unlike traditional EEG monitoring, PPG devices are noninvasive, easy to wear, and allow for continuous monitoring in daily life, which greatly enhances patient compliance. Previous studies^{8,11} have demonstrated that PPG-derived features can effectively capture ANS alterations during seizures, suggesting their potential role as biomarkers for early seizure detection. Our study builds on this evidence by identifying distinct PPG-based features, further supporting their clinical applicability for early seizure detection and personalized epilepsy management.

However, current PPG-based seizure detection systems still face challenges in achieving high accuracy and reliability. Recent research^{9,16–19} has reported that the sensitivity of PPG-based seizure detection systems varies between 32% and 93%, with false alarm rates ranging from 0.04 to 2.3 events per 24 h, underscoring the need for further refinement. A previous study⁹ of a dataset comprising 11 patients and 47 temporal lobe seizures revealed that PPG-based seizure detection achieved a sensitivity of only 32%, which was substantially lower than that of hospital-grade ECG systems (57%). Van Andel et al.⁵ examined PPG measurements from the Empatica wristwatch and compared them with ECG recordings, finding that both spontaneous and seizure-related movements interfered with biosensor performance, limiting its ability to acquire high-quality data. These findings underscore the need for improved methodologies to increase the reliability of PPG-based seizure detection.

Limitations

Despite the promising findings of this study, several limitations should be acknowledged. First, the sample size was relatively small, and the data were collected from a single center, which may limit the generalizability of the results. Therefore, future studies should involve larger sample sizes and multicenter designs to further validate these findings. Second, postural changes can significantly affect PPG signals, introducing variability that may compromise signal accuracy and the reliability of subsequent analysis³⁹. However, in this study, the PPG data were collected during video-EEG monitoring, and patients were generally limited to activities near the bed, which helped minimize the impact of motion artifacts on the data. Third, the device used in this study had a

relatively low sampling rate, which may have limited the resolution of the PPG signal. A higher sampling rate could provide more detailed physiological information and improve the accuracy of feature extraction.

Conclusions

This study highlights the hemodynamic alterations in GTCSs and FIAs via PPG-derived features. Compared with that in the FIAs group, the PPG signal in the GTCS group exhibited earlier changes at 30 min before seizure onset. PUS and Kmax may enhance PPG-based early seizure detection by improving sensitivity and reducing false alarms, potentially increasing its clinical applicability.

Data availability

The datasets generated during the current study are not publicly available due to patient privacy protection but have been provided to the journal for review purposes and are available from the corresponding author on reasonable request.

Received: 18 March 2025; Accepted: 12 May 2025

Published online: 04 June 2025

References

1. Fiest, K. M. et al. Prevalence and incidence of epilepsy: A systematic review and meta-analysis of international studies. *Neurology* **88** (3), 296–303 (2017).
2. Fisher, R. S. et al. Operational classification of seizure types by the international league against epilepsy: position paper of the ILAE commission for classification and terminology. *Epilepsia* **58** (4), 522–530 (2017).
3. Elger, C. E. & Hoppe, C. Diagnostic challenges in epilepsy: seizure under-reporting and seizure detection. *Lancet Neurol.* **17** (3), 279–288 (2018).
4. Beniczky, S. et al. Automated seizure detection using wearable devices: A clinical practice guideline of the international league against epilepsy and the international federation of clinical neurophysiology. *Epilepsia* **62** (3), 632–646 (2021).
5. van Andel, J. et al. Multimodal, automated detection of nocturnal motor seizures at home: is a reliable seizure detector feasible? *Epilepsia Open.* **2** (4), 424–431 (2017).
6. Lazeron, R. H. C. et al. Multimodal nocturnal seizure detection: do we need to adapt algorithms for children? *Epilepsia Open.* **7** (3), 406–413 (2022).
7. Glasstetter, M. et al. Identification of ictal tachycardia in focal motor- and non-motor seizures by means of a wearable PPG sensor. *Sens. (Basel Switzerland)* **21** (18) (2021).
8. Allen, J. Photoplethysmography and its application in clinical physiological measurement. *Physiol. Meas.* **28** (3), R1–39 (2007).
9. Vandecasteele, K. et al. Automated epileptic seizure detection based on wearable ECG and PPG in a hospital environment. *Sens. (Basel Switzerland)* **17** (10) (2017).
10. El Atrache, R. et al. Photoplethysmography: A measure for the function of the autonomic nervous system in focal impaired awareness seizures. *Epilepsia* **61** (8), 1617–1626 (2020).
11. Mohammadpour Tousekani, F. et al. Photoplethysmographic evaluation of generalized tonic-clonic seizures. *Epilepsia* **61** (8), 1606–1616 (2020).
12. van Andel, J., Ungureanu, C., Aarts, R., Leijten, F. & Arends, J. Using photoplethysmography in heart rate monitoring of patients with epilepsy. *Epilepsy Behavior: E&B.* **45**, 142–145 (2015).
13. Jaychandran, R. et al. Monitoring peri-ictal changes in heart rate variability, oxygen saturation and blood pressure in epilepsy monitoring unit. *Epilepsy Res.* **125**, 10–18 (2016).
14. van Westrhenen, A., De Cooman, T., Lazeron, R. H. C., Van Huffel, S. & Thijs, R. D. Ictal autonomic changes as a tool for seizure detection: a systematic review. *Clin. Auton. Res. Off. J. Clin. Auton. Res. Soc.* **29** (2), 161–181 (2019).
15. Safavi, S. M. et al. Analysis of cardiovascular changes caused by epileptic seizures in human photoplethysmogram signal. (2019).
16. Arends, J. et al. Multimodal nocturnal seizure detection in a residential care setting: A long-term prospective trial. *Neurology* **91** (21), e2010–e9 (2018).
17. van Westrhenen, A., Lazeron, R. H. C., van Dijk, J. P., Leijten, F. S. S. & Thijs, R. D. Multimodal nocturnal seizure detection in children with epilepsy: A prospective, multicenter, long-term, in-home trial. *Epilepsia* **64** (8), 2137–2152 (2023).
18. Böttcher, S. et al. Intra- and inter-subject perspectives on the detection of focal onset motor seizures in epilepsy patients. *Sens. (Basel Switzerland)* **22** (9). (2022).
19. Nasser, M. et al. Non-invasive wearable seizure detection using long-short-term memory networks with transfer learning. *J. Neural Eng.* **18** (5). (2021).
20. Amengual-Gual, M., Ulate-Campos, A. & Loddenkemper, T. Status epilepticus prevention, ambulatory monitoring, early seizure detection and prediction in at-risk patients. *Seizure* **68**, 31–37 (2019).
21. Sharma, H. J. B. Heart rate extraction from PPG signals using variational mode decomposition. *Eng. B.* **39** (1), 75–86 (2019).
22. Khan, M. U., Aziz, S., Iqtidar, K. & RJBSP Fernandez-Rojas Computer-aided diagnosis system for cardiac disorders using variational mode decomposition and novel cepstral quinary patterns. *Control* **81**, 104509 (2023).
23. Orini, M., van Duijvenboden, S., Tinker, A., Munroe, P. B. & Lambiase, P. D. (eds) *Association between Photoplethysmography Pulse Upslope and Cardiovascular Events in Over 170,000 UK Biobank Participants*. Computing in Cardiology (CinC). (IEEE, 2022)
24. Xing, X., Huang, R., Jiang, C. & Dong, W. -f. Contribution of timescale patterns to photoplethysmography-based blood pressure estimation. (2023).
25. Krishnan, R., Natarajan, B. B. & Warren, S. Two-stage approach for detection and reduction of motion artifacts in photoplethysmographic data. *IEEE Trans. Bio Med. Eng.* **57** (8), 1867–1876 (2010).
26. Vieluf, S. et al. Peripheral multimodal monitoring of ANS changes related to epilepsy. *Epilepsy Behavior E&B* **96**, 69–79. (2019).
27. Eggleston, K. S., Olin, B. D. & Fisher, R. S. Ictal tachycardia: the head-heart connection. *Seizure* **23** (7), 496–505 (2014).
28. Park, J., Seok, H. S., Kim, S. S. & Shin, H. Photoplethysmogram analysis and applications: an integrative review. *Front. Physiol.* **12**, 808451 (2021).
29. Khan, U. M. *Enabling Novel Applications Through Sensing with Wireless Signals* (North Carolina State University, 2023).
30. Wannamaker, B. B. Autonomic nervous system and epilepsy. *Epilepsia* **26** (1), S31–S39 (1985).
31. Devinsky, O. Effects of seizures on autonomic and cardiovascular function. *Epilepsy Currents.* **4** (2), 43–46 (2004).
32. Haneef, Z. & Matsumoto, J. H. Seizures and epilepsy syndromes. In: (ed Haneef, Z.) *Epilepsy Fundamentals: A Concise Clinical Guide*. Cham: Springer Nature Switzerland; 9–36. (2024).
33. Udhayakumar, R. et al. Measurement of stress-induced sympathetic nervous activity using multi-wavelength PPG. *Royal Soc. Open. Sci.* **10** (8), 221382 (2023).
34. Liu, B. et al. The assessment of autonomic nervous system activity based on photoplethysmography in healthy young men. *Front. Physiol.* **12**, 733264 (2021).

35. Zijlmans, M., Flanagan, D. & Gotman, J. Heart rate changes and ECG abnormalities during epileptic seizures: prevalence and definition of an objective clinical sign. *Epilepsia* **43** (8), 847–854 (2002).
36. Mayer, H. et al. EKG abnormalities in children and adolescents with symptomatic Temporal lobe epilepsy. *Neurology* **63** (2), 324–328 (2004).
37. Scherthaner, C., Lindinger, G., Pötzelberger, K., Zeiler, K. & Baumgartner, C. Autonomic epilepsy—the influence of epileptic discharges on heart rate and rhythm. *Wien. Klin. Wochenschr.* **111** (10), 392–401 (1999).
38. Sevcencu, C. & Struijk, J. J. Autonomic alterations and cardiac changes in epilepsy. *Epilepsia* **51** (5), 725–737 (2010).
39. Zaidi, S., Collins, S. J. B. P. & Express, E. Orthostatic stress and area under the curve of photoplethysmography waveform. **2** (4), 045006. (2016).

Acknowledgements

This work was supported by the Major Program of the National Natural Science Foundation of China (Grant Number 82471476).

Author contributions

A.M. and C.F. contributed to the study conception, study design, data collection, data analysis, manuscript writing, and manuscript revision. Z.L. and Y.Y. contributed to the study design and data analysis. X.W., M.W., J.W., Z.H. and Y.B. contributed to the study design and data collection. L.G. supervised the study, contributed to the study design, manuscript writing, and manuscript revision. All authors reviewed the manuscript.

Declarations

Competing interests

The authors declare no competing interests.

Additional information

Supplementary Information The online version contains supplementary material available at <https://doi.org/10.1038/s41598-025-02127-3>.

Correspondence and requests for materials should be addressed to G.L.

Reprints and permissions information is available at www.nature.com/reprints.

Publisher's note Springer Nature remains neutral with regard to jurisdictional claims in published maps and institutional affiliations.

Open Access This article is licensed under a Creative Commons Attribution-NonCommercial-NoDerivatives 4.0 International License, which permits any non-commercial use, sharing, distribution and reproduction in any medium or format, as long as you give appropriate credit to the original author(s) and the source, provide a link to the Creative Commons licence, and indicate if you modified the licensed material. You do not have permission under this licence to share adapted material derived from this article or parts of it. The images or other third party material in this article are included in the article's Creative Commons licence, unless indicated otherwise in a credit line to the material. If material is not included in the article's Creative Commons licence and your intended use is not permitted by statutory regulation or exceeds the permitted use, you will need to obtain permission directly from the copyright holder. To view a copy of this licence, visit <http://creativecommons.org/licenses/by-nc-nd/4.0/>.

© The Author(s) 2025